Science and Engineering Research Council
Rutherford Appleton Laboratory
CHILTON, DIDCOT, OXON, OX11 0QX

RL-82-053

Computer modelling of e-beam-pumped KrF lasers

C B Edwards, F O'Neill

July 1982

Computer modelling of e-beam-pumped KrF lasers

C B Edwards and F O'Neill

Laser Division, SERC Rutherford Appleton Laboratory,
Chilton, Didcot, Oxon OX11 0QX, UK

Abstract

A computer kinetics model has been developed to predict the steady state behaviour of e-beam-pumped KrF lasers. The model can be used to calculate species densities, gain, loss and efficiency of the laser. Close agreement is obtained between our model and a wide range of experimental measurements of optical gain, loss, and laser efficiency as a function of e-beam pump power, taken at various laboratories.

I INTRODUCTION

A computer kinetic model of the electron-beam pumped krypton fluoride laser has been developed to complement the analysis of recent experimental results on the behaviour of the KrF laser [1], and to aid the design of SPRITE, a 200 joule rare gas halide laser currently under construction at these laboratories [2]. Access to such a model is important due to the complex inter-dependence of the operating parameters of any KrF laser system (pump rate, gas mixture, pressure etc) and the resulting difficulty in optimising such a device. Under our experimental conditions of high pump rate (between 1 and 4 $MWcm^{-3}$) and high gas pressure (up to 2,500 torr total), the characteristic time taken to reach a kinetic equilibrium for the important species in the model is estimated to be of the order of 15 nsec. This is obtained from fig 1; the two slowest rates being the atomic metastable formation reactions from ionic dimers and the ensuing production of excimers , and F_2 quenching of Kr_2F^* and Ar_2F^*. Since the duration of the pumping pulse for the systems of interest to us is$\geq$50 nsec, a steady state approach has been adopted for the kinetic modelling of laser oscillation. The model has been found to be extremely useful in predicting intrinsic efficiency of the laser media, optical gain and loss, and is currently finding applications in the design of SPRITE [2].

There are, however, two principal limitations of the steady state, kinetic equilibrium approach. Firstly, it is not possible to consider oscillator transients due to cavity build-up time, relaxation oscillations etc; secondly the code gives no information of pulse shape modification and propagation due to saturation effects which become important at high intracavity flux in laser amplifiers, and is unable to predict the effect of temporal variations in the pumping pulse.

The overall accuracy of the model is determined by the uncharacterised 'products', as listed for certain reactions in Tables 1-6, which leave the steady-state accounting scheme. This leads to an imbalance in steady state population conservation of approximately 8% for a 50 nsec pulse which is estimated to propagate an error of $\sim$ 5% in all computations. This is well within experimental errors and is not considered important at this stage.

Consequently, comparisons between experiment and the model must be made under conditions in which ASE is not important; this can be inconvenient under certain circumstances since the KrF laser is inherently a high-gain system, but is not a limitation for the present use of the code since we are primarily interested in the simulation of saturated laser amplifiers.

II GENERAL DESCRIPTION OF THE KINETICS MODEL

Fourteen species, which are believed to play an important role in the KrF laser kinetics, are incorporated in the model. These include atomic and molecular ions (F^-, Kr^+, Ar^+, Kr_2^+, Ar_2^+), the rare gas metastables, (Ar^* and Kr^*), and the diatomic and triatomic excimers (KrF^*, ArF^*, Kr_2F^*, $ArKrF^*$, and Ar_2F^*). In total, some fifty reaction processes are simulated including the fomation kinetics of KrF^*, quenching of excited species, radiative and absorptive processes and the metastable reactions. Cross-sections and rate coefficients are taken where possible from the literature and the complete list of reactions and references to the data is shown in Tables 1-6. The rate equations for the population densities of the atomic and molecular species, the intracavity photon flux, and the electron density are solved in steady state by the Gauss elimination method using a matrix formulation for ease of computation. The use of a steady state approximation greatly reduces the amount of computation time required for each calculation; this is important since several of the rate equations are non-linear to second order in the chosen variables. This requires that the population density of KrF^*, F_2, F^-, e^-, and the photon flux are calculated (to any chosen accuracy within the 5% limit of the scheme) by nested iterations, and consequently each solution takes a substantial amount of processor time.

In order to calculate the laser flux, the photon density in the cavity is simply adjusted to sustain the laser on the threshold of oscillation as defined by the equation:

$$R_1 R_2 \exp(2g_o \ell) = 1 \qquad \ldots\ldots\ldots\ldots (1)$$

where R_1, R_2 are the mirror reflectivities, ℓ is the length of the gain medium, and g_o is the net gain coefficient defined by:

$$g_o = \sigma_s [KrF^*] - \sum_i \sigma_a(i) [i] \quad \ldots\ldots\ldots\ldots (2)$$

where σ_s is the KrF^* stimulated emmission cross section at the laser wavelength (249nm), and $\sigma_a(i)$ is the absorption cross section of species (i) at the same wavelength; quantities in square brackets denoteing species population density. It should be noted that equation (1) is most accurate for the case of high Q cavities, when the photon flux is distributed uniformly in the cavity. Thus a small discrepancy is expected to occur since KrF lasers are typically operated with mirror reflectivity products of $\sim$ 15 - 20% due to the high intrinsic gain.

III DETAILS OF THE MODEL

The dominant kinetic processes in the model listed in tables 1-6 are displayed diagrammatically in fig 1. These processes are described below and some comparisons are made with previously published KrF laser models.

(i) Pumping

From fig 1, it can be seen that the primary energy deposition processes are ionisation of argon and krypton atoms, and direct excitation of the metastables Ar^* and Kr^* by high energy electron collision. KrF^* and ArF^* excimers are then formed by the saturated 3-body reactions:

$$R^+ + F^- + M \rightarrow RF^* + M \quad \ldots\ldots\ldots\ldots (3)$$

where R is a rare gas atom and M is a krypton or argon atom in the case of e-beam pumping

or by the neutral, metastable reactions:

$$R^* + F_2 \rightarrow RF^* + F \quad \ldots\ldots\ldots\ldots (4)$$

The average energy lost in an ionising collision between the high

energy electrons in the primary pumping beam (and the associated highly energetic secondaries) and the rare gas atoms, denoted by W, is approximately 26eV for both argon and krypton. In the model it is assumed that for each Wev lost by an electron in a collision with a rare gas atom, one ion pair is formed in the laser gas. In addition, due to the distribution of energy among excited atomic states formed in non-ionising collisions, one rare gas metastable, R^*, is produced for each 3.5Wev[3] deposited in the gas. In this way any chosen pump rate is related to the ion and metastable production rate in the laser medium. The relative pumping between argon and krypton is assumed to be proportional to the respective (density X stopping power) product [4].

(ii) F^- Production

Ion channel production of KrF^* is dependent upon dissociative attachment of electrons to F_2 as in reaction (6) in Table 1 to form the F^- ion. It is clear from the data given in ref [5] that the rate constant for the process is strongly dependent upon electron temperature in the region 0.1eV to 1.0eV, the likely secondary electron temperature range in these systems. In our model, we obtain the best fit to experimental data using a value for the rate constant of $7.5 \times 10^{-9} cm^3 s^{-1}$, corresponding to a secondary electron temperature of 0.75eV. This value of the rate constant is consistent with the value taken for the model described in ref [14], though much larger than that used in ref [24] ($1.1 \times 10^{-9} cm^3 s^{-1}$).

(iii) Absorption Processes

The absorbers treated in the present model are shown in Table 4. We have found that the theoretical predictions of the model are most strongly dependent upon the values of absorption cross-section of Ar_2F^* and Kr_2F^*. The best fit to experimental data is obtained using the following values:

$$\sigma_a (Ar_2^+) = 5 \times 10^{-17} cm^2$$
$$\sigma_a (Kr_2F^*) = 1.3 \times 10^{-17} cm^2$$

Both of these values are somewhat larger than those used in previous model calculations for the KrF laser; however, the value for Ar_2F^* is in good agreement with the values given in ref [6], while the value for Kr_2F^* is within the experimental errors of the value obtained experimentally at this laboratory [1].

IV EXPERIMENTAL RESULTS

The construction of the model was based upon the adjustment of certain parameters where appropriate to obtain agreement with experimental values of optical gain and loss obtained at this laboratory and then subsequent testing of the model with data taken at other laboratories over a wide range of operating conditions without further adjustment to the rate constants. Since the output characteristics of any laser system are fundamentally determined by the optical gain and loss in the active medium, experiments were performed using the electron beam generator at these laboratories [7] to measure these quantities for comparison with the model [1]. Net gain was measured using the single/double pass amplified spontaneous emission technique [8]. Any measurement of absorption of the laser medium at the laser wavelength is impossible, since only net gain can be obtained from optical probing; instead, measurements were made slightly removed from the emission band, since it is believed that the important absorbers, Ar_2^*, Kr_2F^*, F^- exhibit comparatively broad absorption features in the important wavelength region for the operation of the KrF laser. We therefore used frequency doubled 514.5nm radiation from a CW argon ion laser as a probe to measure absorptions at 257.2nm, 8nm to the long wavelength side of the laser gain peak. This is a convenient wavelength experimentally since the KrF^* emission can easily be removed from the absorption signal by modest spectral filtration. The technique outlined above depends upon the absence of line absorbers, but these are not expected to be present under our experimental conditions at this wavelength. A typical record, showing the transient absorption of the u.v. probe, measured with a fast photomultiplier is shown in fig (2).

(i) Comparison with our own experimental measurements

Details of this work have already been reported elsewhere [1]; however, the more important features are summarised below. We have measured gain and absorption in e-beam excited KrF under various

experimental conditions. Variation of gain and loss has been measured as a function of gas mixture and pump rate; prior to this work only spot measurements at fixed pump rate were available. The excitation studies employed a pump rate of 0.5 to 4.5 $MWcm^{-3}$, and the gas mixture chosen was of constant krypton and fluorine pressure, with a variation of argon pressure between 900 torr and 2400 torr. representing the extremes of gas mix used in KrF lasers.

Absorption measurements, at 257.2nm as described above, were made both in the presence of lasing photon flux in the cavity, and under non-oscillating conditions. Typical absorption results are shown in fig 3. From this and other similar data, the contribution to the absorption due to partially interceptible formation of Kr_2F^* has been calculated [1].

The variation of gain as a function of pump rate is shown in fig 4 for three total gas pressures. The experimental conditions were carefully controlled to prevent depletion of gain due to ASE, since this is not treated by the code at this stage. The broken lines are the computed values from the code using input data from Tables 1-6. Fig 5 shows the variation of net gain and loss (with and without laser flux in the cavity) as a function of pump rate.

(ii) Comparison with other data

The code was used to predict the laser performance obtained by other workers as shown in Table 7 [Ref 27, 34, 35]. It will be noted that the agreement is generally good over a wide range of pump powers and gas mixtures, giving confidence in the use of the code to predict the performance of new laser systems, as required for design of SPRITE.

V CONCLUSION AND DISCUSSION

The code predictions for the intrinsic efficiency of the KrF laser (defined as laser output/energy deposited in the gas) have been in close agreement with the experimental values obtained at this and other laboratories over a wide range of operating parameters. It also gives good agreement with the fundamental quantities of optical gain and

loss, and has successfully predicted the saturation of loss as a function of intracavity flux. This is believed to be due to the formation of increased amounts of Kr_2F^* from the high density of KrF^* in the absence of stimulating photon flux.

There is evidence that the KrF B-state is not fully relaxed at the pressures of interest for efficient laser operation, and this would lead to the Kr_2F^* formation saturating in a different way to the optical gain of the medium (since higher vibrational levels in the B-state manifold exhibit a smaller stimulated emission cross section, whilst Kr_2F^* formation is independent of vibrational excitation of KrF^*). This has been observed experimentally [1,10], and must imply a reduction of laser efficiency; however, the intrinsic efficiencies observed are consistent with a simple extraction efficiency argument, based on the ratio of small signal gain to non-saturable loss [11], without added reductions due to inhomogeneous broadening of the laser transition.

At this stage it is difficult to determine the importance of this effect, since the remaining absorption in the medium under conditions in which the lasing transition is heavily saturated will not be totally interceptible due to Kr_2F^*, but will contain components due to F^-, Ar_2^*, etc. A further complication is the formation of Kr_2F^* via chanels which do not involve KrF^*, (via reactions 47 and 40 in Table 6) and are thus non interceptible. It is not believed worth while to attempt a modelling of the vibrational effects in the KrF B-state, since relaxation rates, and hence population distribution in the manifold, are not known to sufficient accuracy; this may be done when reliable rate constants are available since the behaviour of the upper state population is of crucial importance to the short pulse amplification properties of KrF. At the present time, the code is to undergo development to treat time-dependent and spatially varying input data, enabling a full analysis of ASE to be incorporated.

The authors wish to acknowledge helpful discussions with R G Evans and M J Shaw.

References

1. C B Edwards, F O'Neill, M J Shaw
   Appl. Phys. Lett 38, 843 (1981)

2. D Craddock, C B Edwards, F S Gilbert, F O'Neill, D J Nicholas, P Rockett, M J Shaw
   Development of Pulsed E-Beam Systems for Large Volume, High Power, KrF Lasers.
   Proceedings of 4th International Pulsed Power Conference, Albuquerque, New Mexico July 1981 (In Press)

3. D C Lorents
   Physica 82C, 19 (1976)

4. M J Berger and S M Seltzer
   Tables of Energy Losses and Ranges of Electrons and Positrons
   National Aeronautics and Space Administration Report No NASA SP-3012 (1964) (Unpublished)

5. R J Hall
   J. Chem. Phys 68, 1803 (1978)

6. F Collier, J B Leblond, F Hoffbeck, P Cottin
   J. Chem. Phys 74, 4372 (1981)

7. C B Edwards, F O'Neill, M J Shaw
   Appl. Phys. Lett 36, 617 (1980)

8. W E Ernst and F K Tittel
   IEEE J. Quantum Electron QE-16, 945 (1980)

9. J H Jacob, D W Trainor, M Rokni and J C Hsia
   Appl. Phys. Lett 37, 522 (1980)

10. M C Gower and C B Edwards
    Opt. Comm. 40, 369 (1982)

References (Contd)

11. W W Rigrod
IEEE J. Quantum Electron QE-14 377 (1978)

12. E W McDaniel, V Cermak, A Dalgarno, E E Ferguson, L Friedman
Ion-Molecule Reactions, Wiley Interscience, New York 1970 p 338

13. D K Bohme, N G Adams, M Moselman, D B Dunkin, E E Ferguson
J. Chem. Phys. 52, 5094 (1970)

14. J H Jacob, M Rokni, J A Mangano, R Brochu
Appl. Physics Lett. 32, 109 (1978)

15. M R Flannery and T P Yang
Appl. Physics Lett. 32, 327 (1978)

16. J M Wadehra and J N Bardsley
Appl. Physics Lett. 32, 76 (1978)

17. M Rokni, J H Jacob and J A Mangano
Phys. Rev. A 16, 2216 (1977)

18. J N Bardsley and M A Biondi
Adv. Atomic and Molecular Physics 6 (1970)

19. C A Brau
Rare Gas Halogen Excimers
Topics in Applied Physics Vol 30 Editor C K Rhodes, Published by Springer-Verlag

20. W B Lacina and D B Cohn
Appl. Phys. Lett 32, 106 (1978)

21. M Rokni, J A Mangano, J H Jacob, J C Hsia
IEEE J. Quantum Electron QE-14, 464 (1978)

22. J A Mangano, J H Jacob, M Rokni, A Hawryluk
Appl. Physics Lett. 31, 26 (1977)

References (Contd)

23. D W Trainor and J H Jacob
Appl. Physics Lett. 37, 675 (1980)

24. T H Johnson and A M Hunter
J. Appl. Phys. 51, 2406 (1980)

25. H H Nakano, R M Hill, D C Lorents, D L Huestis, M V McCusker
SRI Report No MP-76-99, 1976

26. W R Wadt and P J Hay
J. Chem. Phys. 68, 3850 (1978)

27. A M Hawryluk, J A Mangano and J H Jacob
Appl. Physics Lett. 31, 164, 1977

28. G P Quigley and W M Hughes
Appl. Physics Lett. 32, 650 (1978)

29. L Vriens
Physica 31, 395 (1965)

30. M R Flannery and T P Yang
Appl. Physics Lett. 33, 574 (1978)

31. A Mandl
Phys. Rev. A 3, 251 (1971)

32. R A Haas, W L Morgan
Chapter 7, Laser Program Annual Report 1979
(UCRL-50021-79)
Lawrence Livermore National Laboratory

33. H T Powell Private Communication

34. E L Patterson, J K Rice, G C Tisone
Appl. Physics Letters, 36, 188, 1980

References (Contd)

35. R S Bradford, W B Lacina, E R Ault, M C Bhaumik
Electronic Transition Lasers II
Proceedings of the Third Summer Colloquium on Electronic Transition Lasers, Edited by L E Wilson, S N Suchard and J I Steinfeld, SNOMASS, 1976 (M.I.T., Michigan 1976)

CAPTIONS

Fig 1 Kinetic Process Flow Diagram for Code at 1 $MWcm^{-3}$ Pump Rate (Non Lasing)

Fig 2 Transient Intracavity Absorption
(a) without Laser Oscillation
(b) with Lasing

Fig 3 Absorption at 257.2nm as a Function of Pump Rate and Gas Pressure

Fig 4 Net Gain at 249nm as a Function of Pump Rate and Gas Pressure

Fig 5 Gain and Loss in 1500 torr Gas Mixture

Table 1-6 Kinetic Processes and Rates incorporated in the Code

Table 7 Comparison of KrF Kinetics Model with Experiments

TABLE (1)

PRIMARY KINETICS

	REACTION	RATE	REF.
1	$Ar + e \longrightarrow Ar^* + e_s + e$	26eV/ion pair	3(a)
2	$Kr + e \longrightarrow Kr^* + e_s + e$	24eV/ion pair	3(a)
3	$Ar^* + Ar + Ar \longrightarrow Ar_2^* + Ar$	$2.5 \times 10^{-31} cm^6 s^{-1}$	12
4	$Ar_2^* + Kr \longrightarrow Kr^* + 2Ar$	$7.5 \times 10^{-10} cm^3 s^{-1}$	13
5	$Kr^* + Kr + \binom{Ar}{Kr} \longrightarrow Kr_2^* + \binom{Ar}{Kr}$	$2.5 \times 10^{-31} cm^6 s^{-1}$	14
6	$F_2 + e \longrightarrow F^- + F$	$7.5 \times 10^{-9} cm^3 s^{-1}$	5
7	$Ar^* + F^- \longrightarrow ArF^*$	$3.0 \times 10^{-6} cm^3 s^{-1}$	15(b)
8	$Ar_2^* + F^- \longrightarrow ArF^* + Ar$	$1.5 \times 10^{-6} cm^3 s^{-1}$	16
9	$Kr^* + F^- \longrightarrow KrF^*$	$3.0 \times 10^{-6} cm^3 s^{-1}$	15(b)
10	$Kr_2^* + F^- \longrightarrow KrF^* + Kr$	$1.0 \times 10^{-6} cm^3 s^{-1}$	16,14
11	$ArF^* + Kr \longrightarrow KrF^* + Ar$	$3.0 \times 10^{-10} cm^3 s^{-1}$	32

FOOTNOTES

(a) RELATIVE DEPOSITION BETWEEN REACTION 1 AND 2 WEIGHTED BY DENSITY AND STOPPING POWER (SECTION III (1)

(b) EFFECTIVE 2-BODY RATE OVER DENSITY RANGE OF INTEREST

TABLE (2)

METASTABLE KINETICS

	REACTION	RATE	REF.
12	$Ar_2^+ + e_s \longrightarrow Ar^* + Ar$	$6.7 \times 10^{-7} cm^3 s^{-1}$	18
13	$Kr_2^+ + e_s \longrightarrow Kr^* + Kr$	$6.7 \times 10^{-7} cm^3 s^{-1}$	19
14	$Ar^* + F_2 \longrightarrow ArF^* + F$	$7.5 \times 10^{-10} cm^3 s^{-1}$	20
15	$Ar^* + e_s \longrightarrow Ar^+ + 2e_s$	$2.8 \times 10^{-8} cm^3 s^{-1}$	29
16	$Kr^* + F_2 \longrightarrow KrF^* + F$	$7.2 \times 10^{-10} cm^3 s^{-1}$	19
17	$Kr^* + e_s \longrightarrow Kr^* + 2e_s$	$4.8 \times 10^{-8} cm^3 s^{-1}$	29
18	$Ar + e_s \longrightarrow Ar^* + e_s$	(c)	3
19	$Kr + e_s \longrightarrow Kr^* + e_s$	(c)	3

FOOTNOTE

(c) INCLUDED IN PRIMARY PUMP KINETICS (SECTION III(1))

TABLE (3)

QUENCHING

	REACTION	RATE	REF.
20	$ArF^* + Ar + Ar \longrightarrow Ar_2F^* + Ar$	$4.0 \times 10^{-31} cm^6 s^{-1}$	20
21	$KrF^* + Kr + \binom{Ar}{Kr} \longrightarrow Kr_2F^* + \binom{Ar}{Kr}$	$6.5 \times 10^{-31} cm^6 s^{-1}$	14, 21
22	$KrF^* + 2Ar \longrightarrow ArKrF^* + Ar$	$4.0 \times 10^{-32} cm^6 s^{-1}$	32
23	$ArF^* + e_s \longrightarrow$ PRODUCTS	$2.0 \times 10^{-7} cm^3 s^{-1}$	23
24	$KrF^* + e_s \longrightarrow$ PRODUCTS	$2.2 \times 10^{-7} cm^3 s^{-1}$	23
25	$KrF^* + F_2 \longrightarrow$ PRODUCTS	$8.0 \times 10^{-10} cm^3 s^{-1}$	14

TABLE (4)

ABSORPTION

	REACTION	CROSS-SECTION (cm^2)	REF.
26	$Ar^+ + h\nu \longrightarrow Ar^+ + Ar$	5.0×10^{-17}	6
27	$Kr_2^+ + h\nu \longrightarrow Kr^+ + Kr$	1.0×10^{-18}	20
28	$F^- + h\nu \longrightarrow F + e_s$	5.0×10^{-18}	31
29	$F_2 + h\nu \longrightarrow 2F$	1.5×10^{-20}	20
30	$Ar^* + h\nu \longrightarrow Ar^+ + e_s$	1.0×10^{-19}	24
31	$Kr^* + h\nu \longrightarrow Kr^+ + e_s$	3.2×10^{-20}	24
32	$Kr_2F^* + h\nu \longrightarrow Kr_2F^{**}$	1.3×10^{-17}	1
33	$Ar_2F^* + h\nu \longrightarrow$ PRODUCTS	1.5×10^{-18}	ESTIMATED

TABLE (5)

RADIATION

	REACTION	RATE	REF
34	$ArF^* \longrightarrow Ar + F + h\nu$	$2.4 \times 10^8\ s^{-1}$	25
35	$KrF^* \longrightarrow Kr + F + h\nu$	$1.5 \times 10^8\ s^{-1}$	25,20
36	$Kr_2F^* \longrightarrow Kr_2F + h\nu$	$6.0 \times 10^6\ s^{-1}$	26
37	$KrF^* + h\nu \longrightarrow Kr + F + 2h\nu$	$2.4 \times 10^{-16}\ cm^2$	27
38	$ArKrF^* \longrightarrow$ PRODUCTS $+ h\nu$	$5.0 \times 10^7\ s^{-1}$	25
39	$Ar_2F^* \longrightarrow$ PRODUCTS $+ h\nu$	$5.4 \times 10^6\ s^{-1}$	26

TABLE (6)

TRIMER REACTIONS

	REACTION	RATE	REF.
40	$Ar_2F^* + e_s \longrightarrow$ PRODUCTS	$1.5\times10^{-7} cm^3\ s^{-1}$	33
41	$Kr_2F^* + e_s \longrightarrow$ PRODUCTS	$5\times10^{-8} cm^3\ s^{-1}$	33
42	$Ar_2F^* + F_2 \longrightarrow$ PRODUCTS	$2.5\times10^{-10} cm^3\ s^{-1}$	30
43	$Kr_2F^* + F_2 \longrightarrow$ PRODUCTS	$4.3\times10^{-10} cm^3\ s^{-1}$	28
44	$ArKrF^* + F_2 \longrightarrow$ PRODUCTS	$1.0\times10^{-9} cm^3\ s^{-1}$	25
45	$ArKrF^* + Ar \longrightarrow Ar_2F^* + Kr$	$2.0\times10^{-11} cm^3\ s^{-1}$	22
46	$ArKrF^* + Kr \longrightarrow Kr_2F^* + Ar$	$2.0\times10^{-11} cm^3\ s^{-1}$	22
47	$Ar_2F^* + Kr \longrightarrow ArKrF^* + Ar$	$1.0\times10^{-10} cm^3\ s^{-1}$	25

TABLE (7)

			PARAMETER	EXPT.	MODEL
SANDIA LABS. [34]	900 torr Ar 97 torr Kr 3 torr F_2	E-BEAM PUMP RATE = 1·8 Mw Cm^{-3}	GAIN	17 ± 1% Cm^{-1}	15·5% Cm^{-1}
			LOSS	0·8 ± 0·25% Cm^{-1}	0·7% Cm^{-1}
AVCO. [27]	1072 torr Ar 45 torr Kr 2·5 torr F_2	100 Kw Cm^{-3}	LASER EFFICIENCY	8·5% Cm^{-1}	8% Cm^{-1}
	2136 torr Ar 137 torr Kr 7 torr F_2	50 Kw Cm^{-3}	GAIN	0·3% Cm^{-1}	0·35% Cm^{-1}
			LOSS	0·15% Cm^{-1}	0·1% Cm^{-1}
NORTHROP [35]	1654 torr Ar 415 torr Kr 9 torr F_2	4 Mw Cm^{-3}	GAIN	24% Cm^{-1}	23% Cm^{-1}

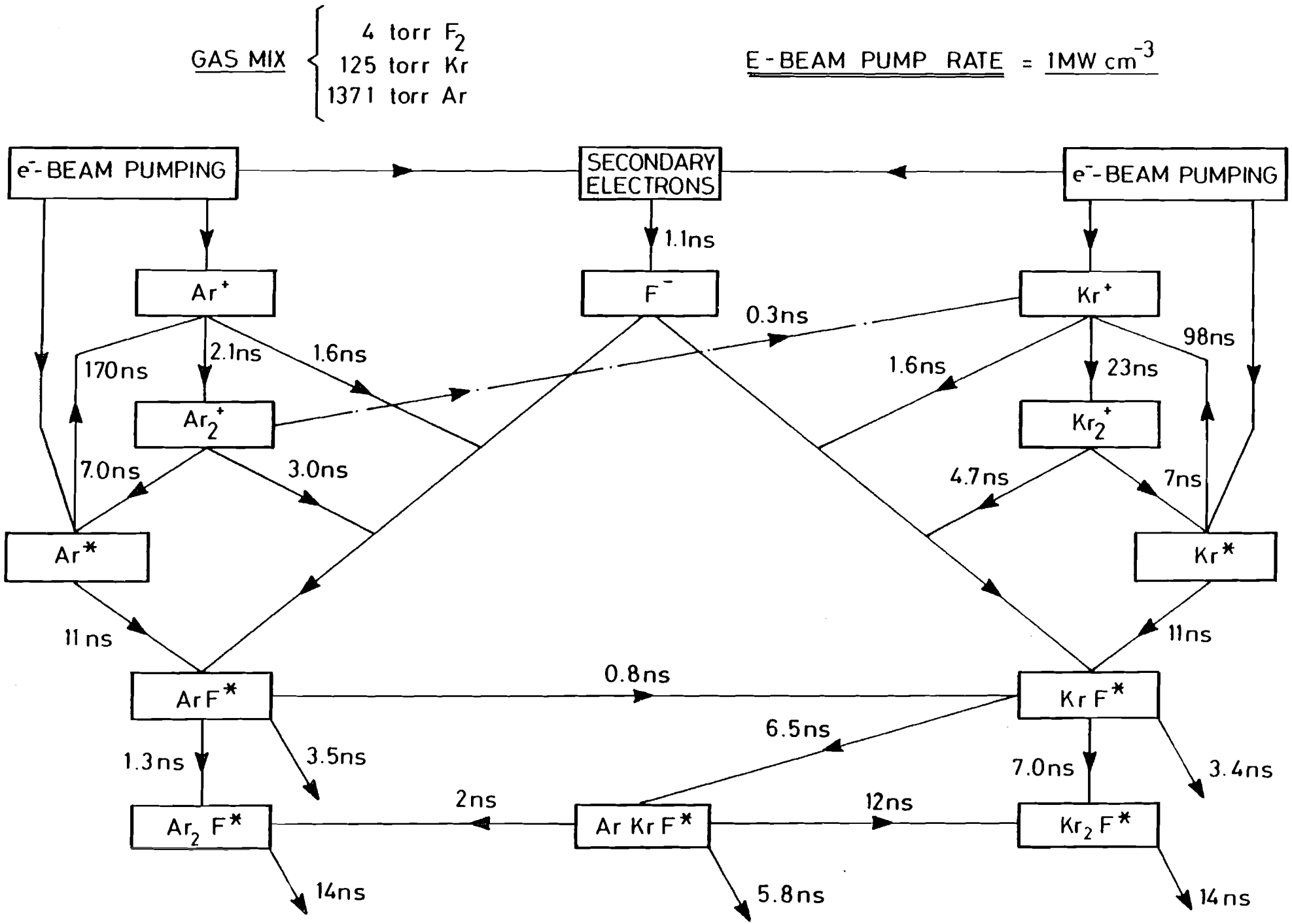
GAS MIX
4 torr F_2
125 torr Kr
1371 torr Ar
E-BEAM PUMP RATE = 1MW cm^{-3}
e$^-$-BEAM PUMPING
SECONDARY ELECTRONS
e$^-$-BEAM PUMPING
1.1ns
Ar^+
F^-
Kr^+
0.3ns
170ns
2.1ns
1.6ns
1.6ns
23ns
98ns
Ar_2^+
Kr_2^+
7.0ns
3.0ns
4.7ns
7ns
Ar*
Kr*
11ns
11ns
ArF*
0.8ns
Kr F*
6.5ns
1.3ns
3.5ns
7.0ns
3.4ns
2ns
12ns
Ar_2 F*
Ar Kr F*
Kr_2 F*
14ns
5.8ns
14ns

FIG (1)

LENGTH OF PUMPED REGION	=	30cm
CW PROBE LASER WAVELENGTH	=	λ = 257.2nm
PEAK E-BEAM PUMP POWER	=	2.1MW/cm^3 (60ns FWHM PULSE)
GAS MIX	=	4 torr F_2 / 125 torr Kr / 1371 torr Ar

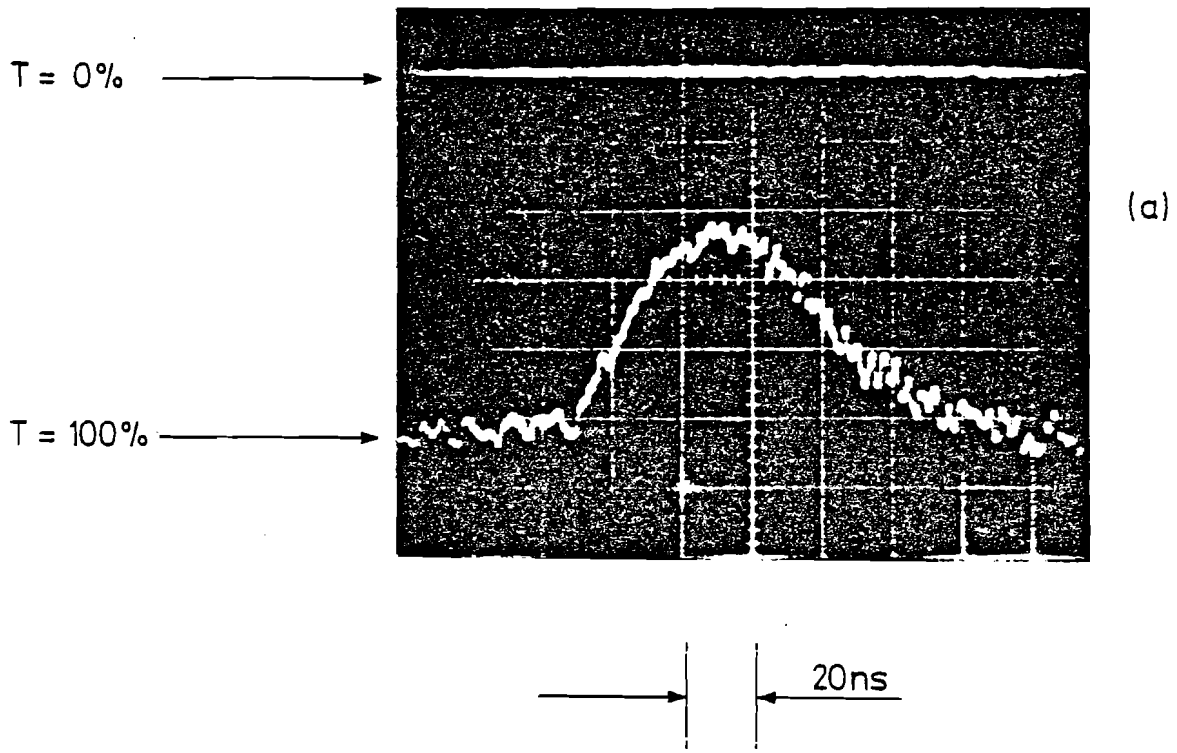

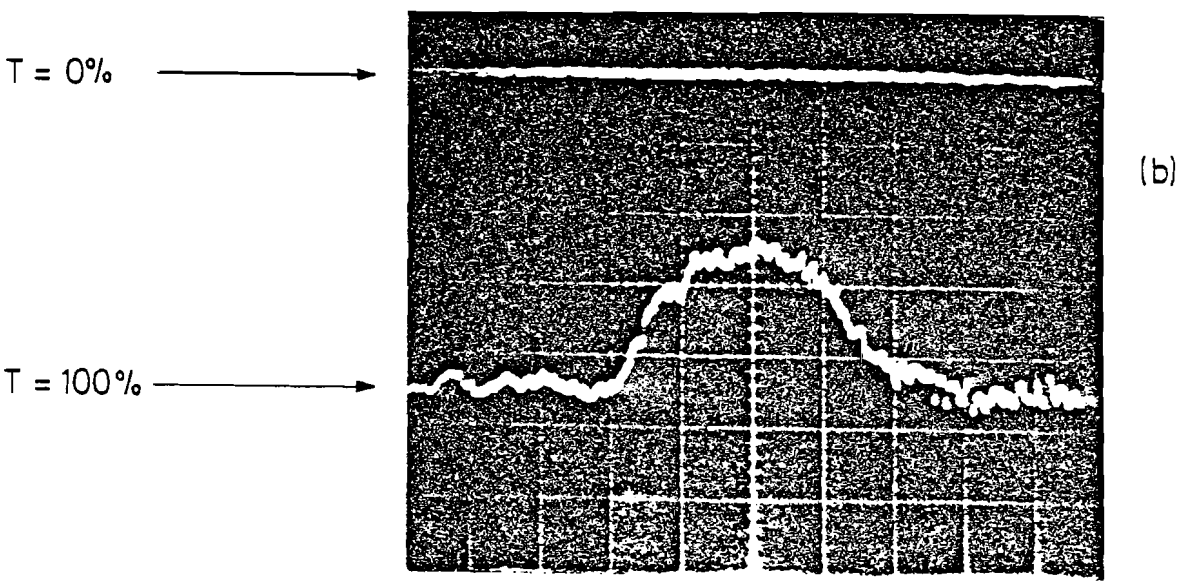

FIG. (2)

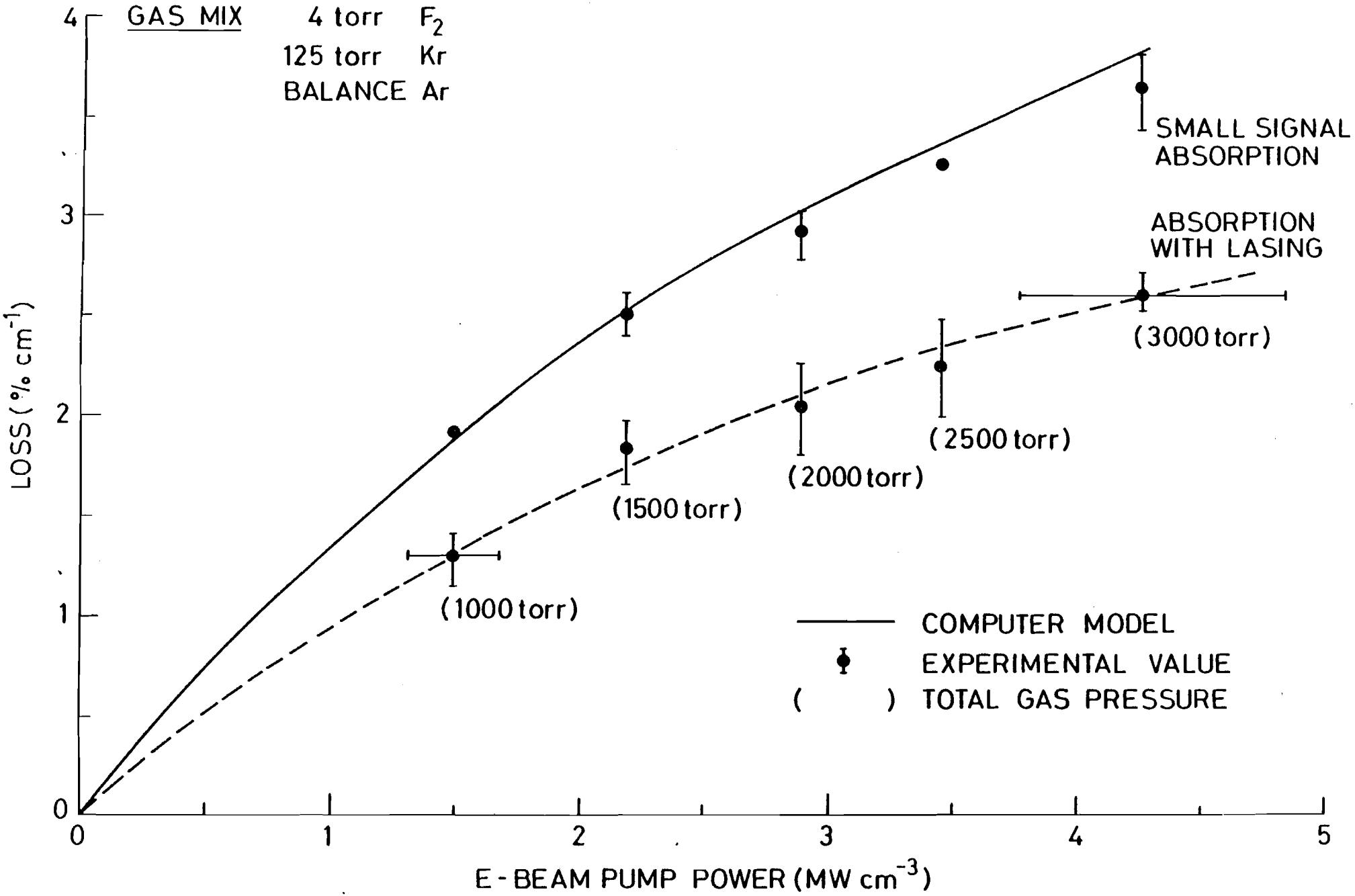
GAS MIX
4 torr F_2
125 torr Kr
BALANCE Ar
SMALL SIGNAL ABSORPTION
ABSORPTION WITH LASING
(3000 torr)
(2500 torr)
(2000 torr)
(1500 torr)
(1000 torr)
COMPUTER MODEL
EXPERIMENTAL VALUE
( ) TOTAL GAS PRESSURE
LOSS (% cm^{-1})
E-BEAM PUMP POWER (MW cm^{-3})
0
1
2
3
4
5

FIG. (3)

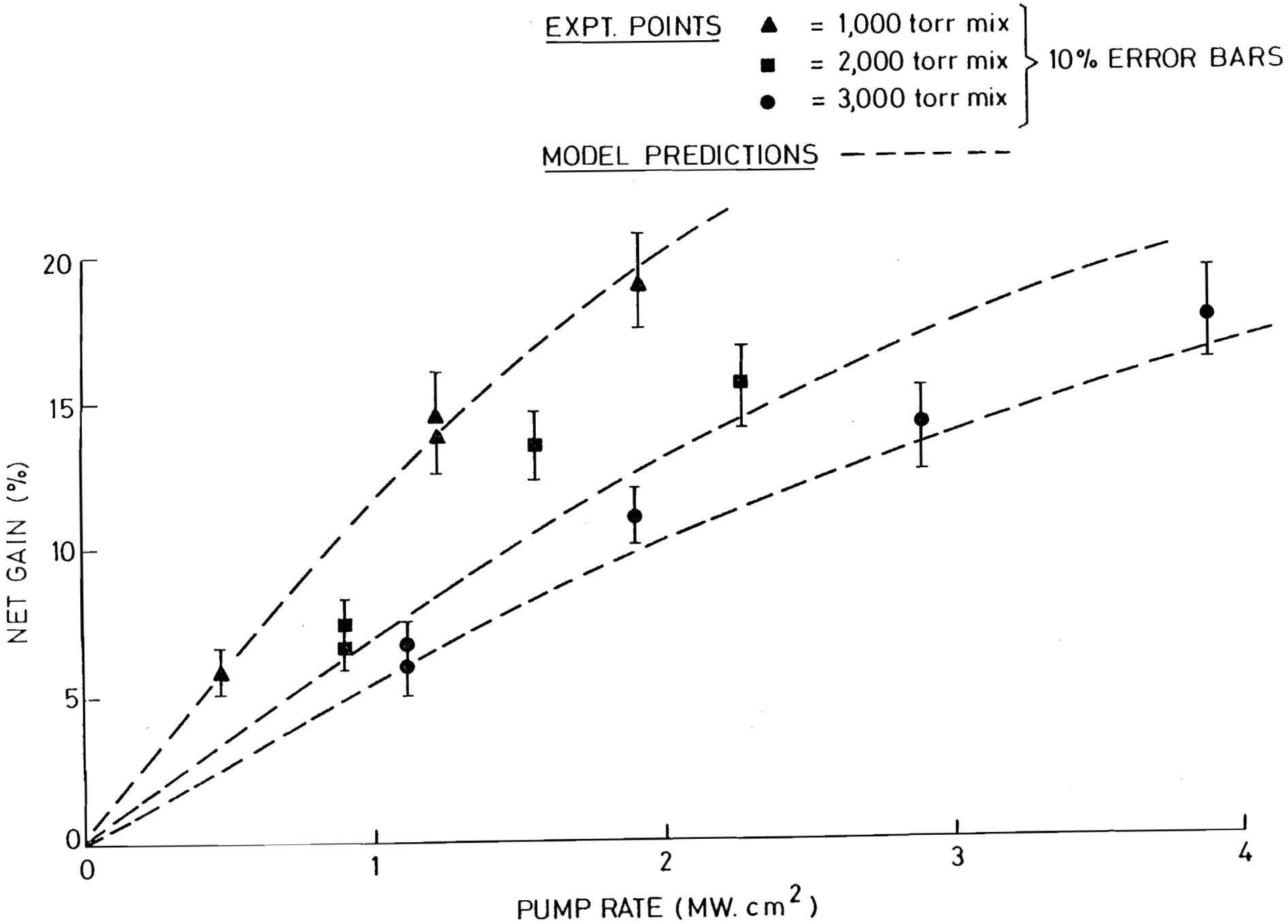
EXPT. POINTS
▲ = 1,000 torr mix
■ = 2,000 torr mix
● = 3,000 torr mix
10% ERROR BARS
MODEL PREDICTIONS
NET GAIN (%)
20
15
10
5
0
0
1
2
3
4
PUMP RATE (MW. cm^2)

FIG. (4)

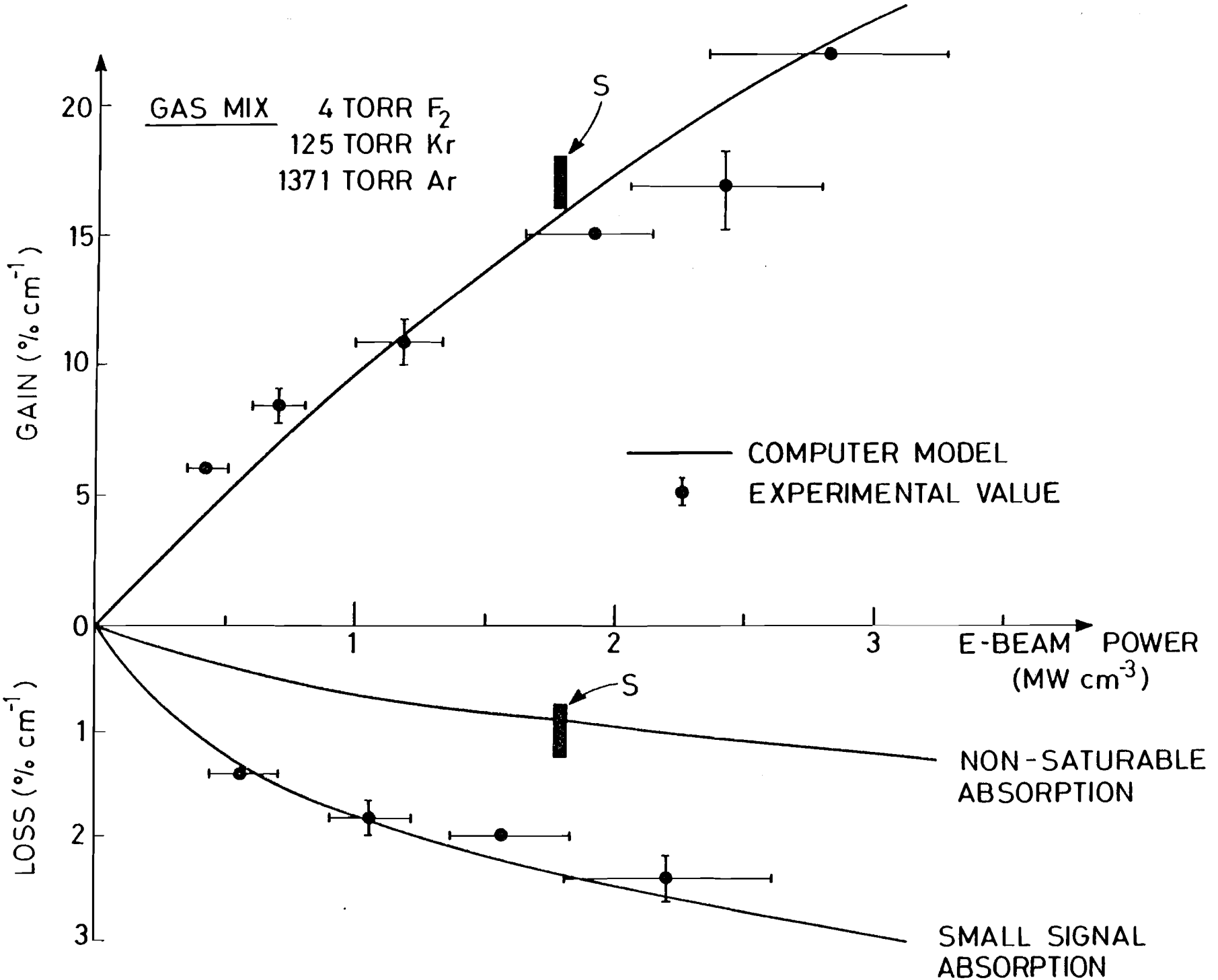
GAS MIX
4 TORR F_2
125 TORR Kr
1371 TORR Ar
S
20
15
10
5
0
1
2
3
GAIN (% cm^{-1})
COMPUTER MODEL
EXPERIMENTAL VALUE
E-BEAM POWER
(MW cm^{-3})
S
1
2
3
LOSS (% cm^{-1})
NON-SATURABLE
ABSORPTION
SMALL SIGNAL
ABSORPTION

FIG.(5)